Strategie di adattamento e patrimonio critico. / Adaptive strategies and critical heritage

Architecture on Demand Design for High-Capacity Optical SDM/TDM/FDM Switching

Miquel Garrich, Norberto Amaya, Georgios S. Zervas, Juliano R. F. Oliveira, Paolo Giaccone, Andrea Bianco, Dimitra Simeonidou and Júlio César R. F. Oliveira

***Abstract*—Reconfigurable optical add/drop multiplexers (ROADMs) are key elements in operators' backbone networks. The breakthrough node concept of Architecture on Demand (AoD) permits to design optical nodes with higher flexibility with respect to ROADMs. In this work, we present a five-step algorithm to design AoD instances according to some given traffic requests, able to support from sub-wavelength time-switching up to wavelength/super-channel/fiber switching. We evaluate AoD performance in terms of power consumption and number of backplane optical cross-connections. Furthermore, we discuss trade-offs involved in the migration from fixed to flexible grid with regard to the optical node size, capacity and power consumption. We compare several ROADM architectures proposed in the literature with AoD in terms of power consumption and cost. We also study different technologies to enhance the scalability of AoD. Results show that AoD can bring significant power savings compared to other architectures while offering a throughput of hundreds of Tb/s.**

***Index Terms*—Optical architectures; switching; routing.**

I. Introduction

INTERNET traffic has been growing fast over the last years due to the emergence of new bandwidth-hungry services supported by new broadband access technologies, both wireless and based on Fiber-To-The-x (FTTx) paradigm. Network operators' infrastructure must support this increasing bandwidth demand while maintaining reasonable levels of QoS, reliability and power consumption in all segments of their network (access, metro and core). To this aim, network operators are attempting to overcome this challenge by increasing their electronic infrastructure and deploying new transmission and switching equipment. However, this solution may pose future interconnection issues on backbone optical networks and may increase operators' OPEX and global CO_2 emission. Enabling flexible-grid spectrum allocation [1], [2] has been devised as the solution to handle both legacy low bitrates and future high-speed super-channels exploiting the available bandwidth in already deployed optical fibers. Therefore, future optical nodes will require to support variable channel bandwidths in a flexible-grid manner so as to achieve higher spectral efficiency. Despite the existence of several proposals of node architectures, mainly based on spectrum selective switches (SSSs), the Architecture on Demand (AoD) approach is motivated by the two following observations.

On the one hand, recently proposed optical node architectures present several limitations. Fig. 1(a) shows the usual reconfigurable optical add/drop multiplexer (ROADM) based on a broadcast-and-select configuration [3]–[5], for which different architectures were proposed. ROADMs are usually dimensioned by N input/output ports (i.e. degree) to provide connectivity with other ROADMs in the network and L add/drop ports (i.e. transponder or client interfaces) for light-paths with local source or destination. These architectures offer the so called Colorless/Directionless/Contentionless (C/D/C-less) features: Colorless means that transponders are not associated to a specific wavelength, Directionless implies that transponders are not associated to a specific input or output port of the node, and Contentionless means that wavelength contention inside the node is eliminated. Interestingly, C/D/C-less capabilities reduce the need of a manual intervention by a technician, compared with the first generations of ROADMS [6]. However, they still present three major drawbacks. First, they offer a limited *flexibility* since they are usually based on a hard-wired arrangement of devices which prevents their upgradeability and their adaptation to new network requirements. Second, they also lack *scalability* in providing a per-service-granularity (i.e. degree, port, waveband or wavelength). In particular, these architectures are constrained by the number of required devices and by their port count. Third, the non-adaptable nature of ROADMs implies high *power consumption*. Indeed, some components of these systems contribute to power consumption regardless of the traffic variations or network requirements (e.g. common equipment in case of ROADMs [7] or O/E/O devices in some optical cross-connect architectures [8]).

On the other hand, unlike other architectures reported in the literature, AoD dynamically synthesizes architectures suited to the switching and processing requirements of traffic [9], [10]. Fig. 1(b) depicts the implementation of AoD consisting of an optical backplane (e.g. 3D-MEMS) that interconnects inputs, outputs, single device modules (e.g. MUXs, couplers, spectrum selective switches (SSSs)) and composed

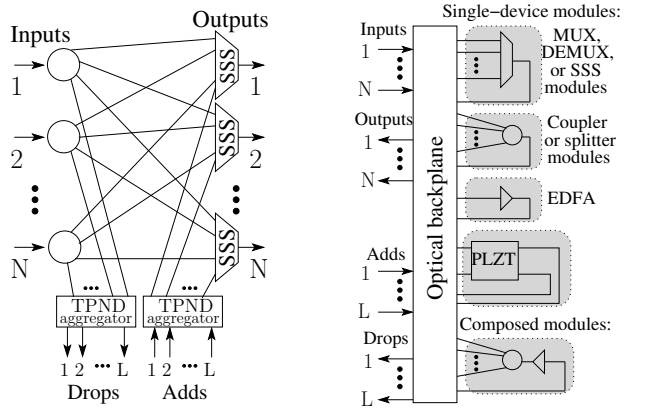

(a) Conventional ROADM (b) AoD implementation

Fig. 1. Conventional ROADM and AoD implementation

Miquel Garrich, Juliano R. F. Oliveira and Júlio César R. F. Oliveira are with CPqD — Centro de Pesquisa e Desenvolvimento em Telecomunicações, Campinas, Brazil.

Paolo Giaccone and Andrea Bianco are with Dipartimento di Elettronica e Telecomunicazioni, Politecnico di Torino, Italy.

Norberto Amaya, Georgios S. Zervas and Dimitra Simeonidou are with High-Performance Networks group, University of Bristol, U.K.

modules (e.g. EDFA + splitter). AoD devotes a subset of the optical backplane ports for local add and drop ports (i.e. L add/drop ports for transponders are considered in the dimensioning of the optical backplane). AoD implements a specific architecture by interconnecting suitable modules by means of the backplane cross-connections to satisfy traffic demands. Together with its inherent flexibility, AoD also pose new challenges some of which are addressed in this work.

The major contributions in this paper are i) a five-step based synthesis algorithm to automatically design and configure AoD instances supporting sub-wavelength time-switching requests, ii) a performance analysis in terms of power consumption and number of backplane optical cross-connections and iii) the study of different technologies to enhance the scalability of AoD. With these contributions we demonstrate the feasibility of implementing AoD nodes with throughput capabilities up to hundreds of Tb/s while providing power consumption savings with respect to usual ROADMs. Preliminary results were presented in [11], [12].

The remainder of the paper is organized as follows. In Sec. II, we consider related works in the literature of ROADMs and AoD. Sec. III details the AoD model and the traffic request. Sec. IV presents a synthesis algorithm for the AoD composition. In Sec. V, we study the performance in terms of scalability and power consumption of AoD over the C band. Furthermore, we discuss the trade-offs between the number of backplane cross-connections, power consumption and throughput for the migration from fixed grid towards flexible allocation of spectrum. Finally, we compare the power consumption of AoD with other architectures. In Sec. VI, we study different technologies to enhance the scalability of AoD. Conclusions are presented in Sec. VII.

II. Related work

In this section we review the related work of ROADM architectures and previous works on Architecture on Demand.

A. ROADMs

Optical networks experienced an enormous evolution over the past 30 years [6]. Thus, being ROADMs key elements in optical networks, their design has been source of numerous studies in the recent literature. The majority of the related works investigate different architectures to achieve colorless, directionless, and more recently, contentionless (CDC) features. Even if the design of ROADMS that guarantee CDC is outside the scope of this work, it is worth to mention the most relevant works on this topic.

The first reference of the colorless feature was done by Basch *et al.* in [13] and the directionless feature was firstly referred by Kaman *et al.* in [14]. The majority of the works since then address a feasibility and scalability comparison of different ROADM alternatives in terms of cost or optical impairments. Among them, [15] can be considered as the first work using this comparison approach. In particular, [15] analyses the scalability of several ROADM architectures composed of 3D-MEMS, wavelength blockers and wavelength selective switches (WSSs). In [16], different architectures are compared in terms of estimated cost considering the use of WSSs and optical 3D-MEMS switches. Similarly, in [3] six ROADM architectures composed of couplers/splitters, (DE)MUXs, WSSs and optical switches are compared in terms of optical impairment and hardware size. In addition, the architectural solutions that guarantee contentionless performance are also discussed. Finally, Gringeri *et al.* in [4] survey ROADM architectural trends for CDC features.

A notable breakthrough for the ROADM design has been the introduction of the planar lightwave circuit (PLC)-based multicast switch (MCS) [17]. More in detail, the MCS provides broadcast-and-select functionality by means of a first stage of N $1 \times M$ splitters connected to a second stage of M $1 \times N$ switches in a relatively small hardware footprint. Different works have analyzed the use of MCS to guarantee completely contentionless performance [18], [19]. It is also worth to mention recent works that analyze different trade-offs between WSS-based and MCS-based ROADMs in terms of optical impairment, cost and power consumption [20], [21].

All the works previously referred propose ROADM node architectures based in a hard-wired connection of devices. Therefore, all the reported architectures may present scalability, flexibility and power consumption drawbacks.

B. Architecture on Demand

The optical node concept of Architecture on Demand was introduced by Amaya *et al.* in 2011 [9]. After that, experimental demonstrations shown that AoD offers complex optical processing functionalities which are outside of the scope of this work. First, in the case that an optical signal requires amplification (e.g. due to through losses) an EDFA module can be added to the particular AoD instance [22]. Second, AoD can include spectrum defragmentation modules to avoid possible wavelength contention issues. More in detail, when two signals from different inputs and at the same spectrum slot request the same output, a wavelength conversion operation must be applied to one of them [23]. More recently, AoD has also been experimentally demonstrated in a software defined networking (SDN) scenario [24] and in a multitechnology/multirate metropolitan/edge scenario [25].

AoD has been shown to provide considerable gains in terms of scalability [11], power consumption [12] and resiliency [26]. More in detail, the work done in [11] and [12] by the same authors is extended here i) presenting a five-step synthesis algorithm for AoD that supports sub-wavelength time-switching requests, ii) a performance analysis in terms of power consumption and number of backplane optical cross-connections and iii) studying space division multiplexing (SDM) and wide available spectrum alternatives to enhance the scalability of AoD in terms of supported throughput.

III. AoD and Traffic Request Models

We focus on a multi-dimensional fiber, super-channel, wavelength and time switching scenario where a high-layer network control plane provides the switching requests of the input signals. In the case of fiber switching, all the signals corresponding to a specific input port are sent towards a destination output, without any spectrum operation. In the case of wavelength channels occupying a single spectrum slot, optical processing is performed by means of fixed-grid Array Waveguide Grating (AWG)-based (DE)MUXs or liquid crystal on silicon (LCoS)-based spectrum selective switches (SSSs) [27]. We allow also super-channel switching, in which a set of contiguous spectrum slots are used to accommodate high-speed channels, e.g. 400 Gb/s, 1 Tb/s and beyond. Time switching allows to implement sub-wavelength time-sliced

channels, in which many channels are multiplexed on the same wavelength in time, according to a predefined TDM scheme. In case of time switching operation, the signal on a wavelength corresponding to a particular timeslot is sent to the destination output, without changing its temporal position. We assume that all the all sub-wavelength time-sliced channels are fully synchronized. Note that a time slot duration of 18 μs was shown experimentally feasible in [23].

Inspired by the AoD implementation of Fig. 1(b), we developed a three-stage logical model, where the use of a module by an optical signal is considered as an AoD stage. In more detail, an optical signal fed in an input port can be switched via the optical backplane either towards an output port or towards a module. If a module is chosen, its output(s) is switched again via the optical backplane either towards an output port or towards a successive module. This process can be repeated up to three modules, i.e. passing through three stages. The output of the third module is always switched via the optical backplane towards an output port. Note that this three-stage model enables most of the required functionalities of current state-of-the-art elastic optical node architectures. In more detail, in [10], Amaya *et al.* describe and analyse four different elastic optical node architectures: "broadcast and select" (2 stages), "spectrum routing" (2 stages), "switch and select with dynamic functionality" (3 stages), and Architecture on Demand. At least two stages are needed to provide wavelength switching towards different destinations: demultiplexing and multiplexing. Moreover, if additional functionality is required (e.g. time switching), then three stages are sufficient. This fact motivates our choice of considering architectures with at most three stages.

Fig. 2 depicts the logical model of the AoD node in which the input ports are connected to the output ports either just through the optical backplane, or through 1, 2 or 3 stages. Let N denote the *degree* of the architecture, i.e. the number of input and output ports. For instance, when input signals require both spectrum and time switching, the first stage performs spectrum routing by means of DEMUXs or SSSs, the second stage performs time-switching by means of 10-ns Piezoelectric Lead lanthanum Zirconate Titanate (PLZT) [28] switches and the third stage couples or MUXes the output signals when needed.

Let W be the number of available spectrum slots per fiber. For example, $W = 96$ for C band DWDM systems with channel spacings of 4×12.5 GHz or $W = 48$ for spacings of 8×12.5 GHz [29].

The *request set* defines the switching requests, that can be any of the following ones:

- A fiber that must switched from an input to an output port.
- A fixed-grid wavelength that must switched from an input to an output port.
- A super-channel that must be switched from an input to an output port.
- A sub-wavelength time-sliced channel that must be switched from an input to an output port, without changing its timeslot.

We assume that the request sets are *feasible* i.e. no output contention is experienced: at most one fiber/wavelength/super-channel must be destined for each output. In the case of sub-wavelengths switching, for each output at most one wavelength must be associated to each timeslot.

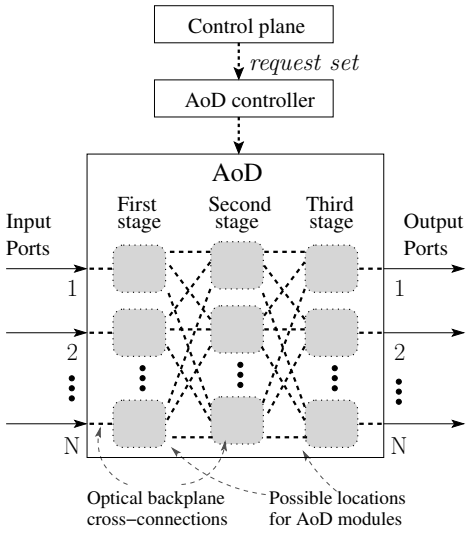

Fig. 2. AoD logical model

A. AoD Backplane Architectures

In order to support heterogeneous traffic requests that may require different types of optical processing (e.g. space/frequency/time switching as in [23]), there is a need of an optical backplane with a high port count. However, available commercial 3D-MEMS optical switches offer up to 320 ports [30] (i.e. two fiber terminations per port: transmit and receive), thus limiting to this maximum the number of backplane cross-connections of the AoD instances and the number of pluggable building modules. Therefore, several optical backplane switches must be interconnected together to overcome this limitation. Relevant to the backplane architectures and the synthesis of AoD instances, we consider the following two definitions:

- *Supported* cross-connections are the optical ports available in the AoD optical backplane (i.e plug-in optical interfaces) for inputs, outputs, adds, drops and modules.
- *Required* cross-connections refer to the set of optical circuits to be established in the AoD optical backplane to properly satisfy a given request set. These optical circuits can be described by pairs of input and output ports according to the request set.

To better understand these definitions, note that when a single optical switch is considered as optical backplane, the number of supported cross-connections coincides with the port-count size of that switch. For instance, 320 cross-connections are supported by an optical backplane built with a single 3D-MEMS optical switch of 320 ports [30]. However, when several switches are interconnected together to compose a larger optical backplane (i.e. using a certain amount of switches' ports for their interconnectivity) the number of supported cross-connections is lower than the sum of all switches' ports. By construction, the required cross-connections must be lower or equal than the supported cross-connections in order to enable the synthesis of AoD instances. Indeed, the required cross-connections derive from the dynamic use of AoD and are the outcome of the Enhanced Synthesis Algorithm (E-SA, see Sec. IV).

In the following, we review two backplane architectures reported in [31].

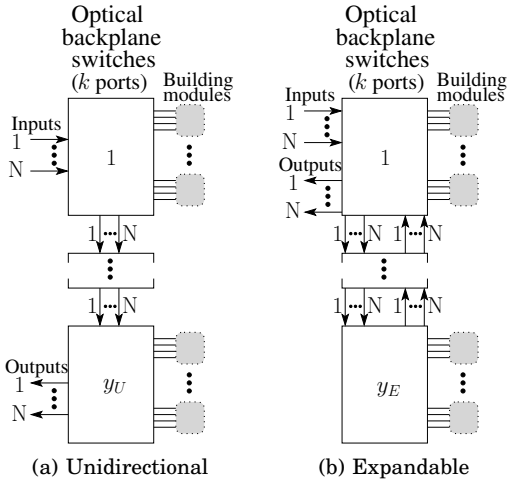

(a) Unidirectional (b) Expandable

Fig. 3. Two alternative architectures for backplane composition

On the one hand, Fig. 3(a) depicts the first architecture, providing a simple approach to solve the backplane port count limitation issue where y_U optical switches of k ports are connected in a unidirectional fashion. In more detail, the N input ports of AoD are connected to the first optical backplane switch. Successive optical backplane switches are connected using N ports until the last (y_U) optical backplane switch, at which all the output ports are connected. Note that optical signals are constrained to pass through all the optical backplane switches. This configuration offers a number of supported cross-connections equal to:

$$X_U = y_U k - N(y_U - 1). \tag{1}$$

Note that for this backplane architecture the number of backplane switches y_U must be set in a resource dimensioning study carried out before AoD is deployed and used. More in detail, once y_U is set and AoD is operating, the connection of additional backplane switches compromises already established optical links through AoD.

On the other hand, Fig. 3(b) depicts the expandable backplane architecture where y_E optical backplane switches of k ports are bidirectionally connected. The N input and output ports of AoD are connected to the first optical backplane switch and $2N$ connections (N in each direction) are set between successive backplane switches. Once AoD is operating, this architecture uses the optical backplane switches in an incremental manner since switches near input and output ports are the first ones to be completely used. Therefore, this expandable backplane architecture allows to tailor y_E to the traffic request and the connection of additional backplane switches without compromising already established optical links through AoD. This configuration offers a number of supported cross-connections equal to:

$$X_E = y_E k - 2N(y_E - 1). \tag{2}$$

Tab. I details the number of supported cross-connections for both backplane architectures considering X_U and X_E according to (1) and (2) respectively for $N = 20$ and $k = 320$; the latter value has been taken equal to a commercially available 320-port 3D-MEMS switch [30]. The adaptable nature that characterizes the expandable backplane architecture allows to increase in a step-wise fashion the number of backplanes y_E (≤ 5 in this example) to satisfy the required cross-connections. This offers a clear benefit for resource dimensioning purposes since additional optical backplane switches may be turned on only when required. On the other hand, for certain values of supported cross-connections (e.g. $1160 \leq X \leq 1220$ and $1440 \leq X \leq 1520$) a higher number of backplane switches is required by the expandable composition compared to the unidirectional backplane composition. Indeed, the unidirectional architecture offers more supported cross-connections for a given number of backplane switches due to the lower number of ports used to interconnect them. However, the unidirectional case requires a preliminary backplane dimensioning study in order to set a constant number of switches y_U.

TABLE I
AVAILABLE CROSS-CONNECTIONS FOR $N = 20$ AND $k = 320$

# switches	Expandable	Unidirectional
1	320	320
2	600	620
3	880	920
4	1160	1220
5	1440	1520

The expandable backplane composition offers two additional advantages compared to the unidirectional composition. Firstly, given a number of backplane switches used in both compositions, i.e. by setting $y_E = y_U \geq 2$, the expandable case permits an arbitrary utilization order of the building modules that belong to different backplane switches whereas in the unidirectional case this would not be possible. Secondly, more than one backplane switch can be connected to the backplane switch with the input and output ports in order to compose a tree-like expandable backplanes. These solutions may present different reachabilities (i.e. number of backplane switches that the optical signals need to go through) of the building modules that belong to different backplane switches while supporting the same number of cross-connections as (2) which corresponds to the expandable composition of Fig. 3(b). However, these tree-like based architectures may be equivalent from the performance point of view to the ones considered in this work, or their possible advantages are limited. Their investigation is left for future work.

In the remainder of the paper we consider the expandable backplane composition due to the highlighted benefits. Therefore, by rearranging (2), the number of backplane switches y_E can be obtained from the number of required cross-connections $X > 2N$ as

$$y_E = \lceil (X - 2N)/(k - 2N) \rceil. \tag{3}$$

B. Example of an AoD Instance

Consider the request set shown in Fig. 4(a), referring to a scenario with $N = 4$ ports and $W = 5$ spectrum slots, with corresponding wavelengths $\lambda_1, \ldots, \lambda_5$. We assume that, for the sub-wavelength channels (denoted as TDM 1,2,3), two slots are present in the frame. The numbers in the figure denote the destination port; in the case of sub-wavelength channels, the couple of numbers denotes the destination port for odd and even slots, respectively, as shown in detail in Fig. 4(b). The considered request set consists of a heterogeneous traffic scenario with six fixed-grid wavelength channels, three sub-wavelength channels and two super-channels.

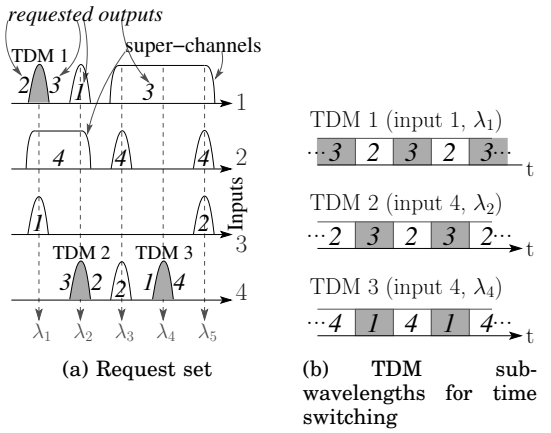

(a) Request set

(b) TDM sub-wavelengths for time switching

Fig. 4. Example of heterogeneous request set with wavelength, super-channel and time switching

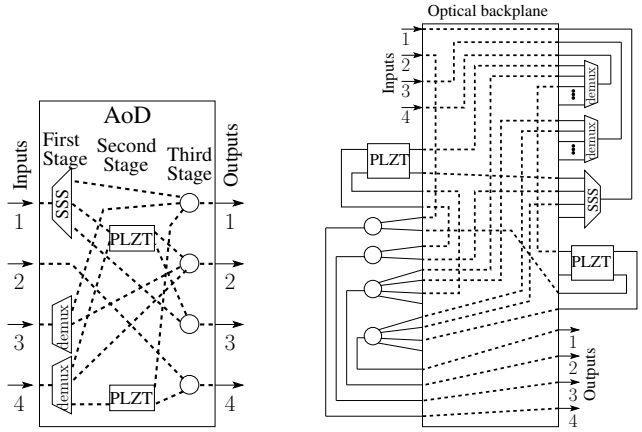

(a) Example of AoD logical instance

(b) Example of AoD instance implementation

Fig. 5. Example of AoD (a) logical instance and (b) its implementation

Fig. 5(a) shows the logical model of a possible AoD configuration satisfying the request set shown in Fig. 4. Channels at input port 1 are fed to a 1×4 SSS to allow flexible spectrum switching, thereby supporting the super-channel. All the channels at input port 2 must be switched to output port 4, thus a single cross-connection is set to the third stage bypassing stages 1 and 2. Two DEMUXs are placed at the first stage of inputs 3 and 4 since channels require to be demultiplexed. At the second stage, two PLZTs are placed to provide the fast time-switching functionality required by inputs 1 and 4, considering a possible reuse of the PLZT optical switch. Note that, in this example, the number of hardware devices (modules) required is 9 and the number of cross-connections is 20, since 13 cross-connections are required for inter-stage connections, 7 to connect both the 3 inputs to the first stage and the 4 outputs to the corresponding modules (or inputs).

Fig. 5(b) shows an AoD implementation (i.e. a schematic of how devices and cross-connections are set and devices are attached to the optical backplane) for the request set shown in Fig. 4. For simplicity, only the used modules are shown. To improve adaptability to future request sets, idle ports of a module are connected to the backplane switch, even if they are unused for the current request set. The process required

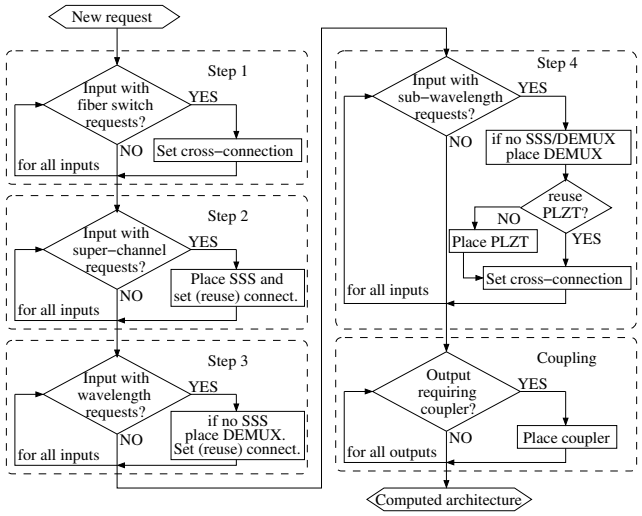

Fig. 6. Flow chart of the Enhanced Synthesis Algorithm (E-SA)

to choose each building module for each position (i.e. the architecture design) according to the request set is explained in the following Sec. IV.

IV. Enhanced Synthesis Algorithm for AoD

We propose the Enhanced Synthesis Algorithm (E-SA) executed at the AoD controller to compute the AoD design based on a given feasible request set. E-SA (whose flow chart appears in Fig. 6) is divided in five steps: four steps perform switching functionalities from coarser to finer granularities (i.e. at fiber, super-channel, wavelength and sub-wavelength level) and the fifth step couples signals from different sources.

In more detail, given a request set, the *first step* checks the destination of all signals from each input. In the case that they are all destined to the same output, a cross-connection is set (e.g. input port 2 in Fig. 5(a)).

The *second step* checks the presence of super-channel requests for each input. If super-channel requests are found, a SSS is placed and a possible reuse of cross-connections is considered (due to the SSS arbitrary bandwidth switching capability), otherwise the required connections are placed (e.g. input port 1 of Fig. 5(a)).

The *third step* checks the presence of fixed-grid wavelength channels to be switched for each input. It may reuse SSS and connections that have been already placed. Otherwise, a DEMUX and the required cross-connections are setup. For the example shown in Fig. 5(a), in this step a cross-connection is set for the wavelength channel at λ_2 at input 1 with destination output 1, and two DEMUXs with the required cross-connections are set for input ports 3 and 4.

The *fourth step* checks the presence of sub-wavelength time-sliced channels for each input. In such a case, a possible reuse of already placed SSS, DEMUXs and cross-connections is considered. Otherwise, a DEMUX is placed if needed. Subsequently, a possible reuse of already placed PLZTs is considered to provide time switching towards the same two required outputs. In the case that the two destinations of the sub-wavelength time slices is not being addressed by an already placed PLZT, a new PLZT is placed to perform time switching between the two required outputs.

In order to better explain this last step of the algorithm, let us recall the example depicted in Fig. 4. Note that this step is executed three times (one for each time-sliced sub-wavelength signal: TDM 1, 2, and 3). In the first execution, according to TDM 1, the upper PLZT of Fig. 5(a) is placed and three cross-connections are set: SSS towards upper PLZT, upper PLZT towards coupler at output 2 and upper PLZT towards coupler at output 3. In the second execution, considering TDM 2, only a cross-connection from the DEMUX at input 4 towards the upper PLZT is set. Note that the upper PLZT can be used by TDM 1 and TDM 2 because both time-sliced sub-wavelengths are switching time slices towards the same two outputs alternately. In the third execution, since the sub-wavelength time-slices of TDM 3 are not being addressed (and available) by any already placed PLZT, the lower PLZT of Fig. 5(a) is placed and three cross-connections are set: DEMUX at input 4 towards lower PLZT, lower PLZT towards coupler at output 1 and lower PLZT towards coupler at output 4.

Finally, the *fifth step* couples at each output the signals from different sources.

This proposed E-SA outperforms our previous synthesis algorithm presented in [11] because it supports sub-wavelengths time-sliced requests in the architecture design. Furthermore, unlike the previous version, E-SA computes only once the coupling of signals required at each output port. Indeed, this guarantees a faster execution time maintaining its complexity $\Theta(N)$.

V. AoD Performance in C Band

In this section we analyze AoD performance in terms of required backplane cross-connections and power consumption when supporting C band DWDM requests with $W = 96$ spectrum slots, thus considering channel spacings of 4×12.5 GHz [29]. To this aim, we generate request sets with the following four parameters.

1) The *port load* $P \in [0,1]$ is the fraction of the requested fixed-grid wavelengths per input over W (i.e. 4×12.5 GHz bandwidth channels).
2) The *sub-wavelength index* $\sigma \in [0,P]$ is the fraction over W of the requested wavelengths per input that contain TDM sub-wavelength signals. We consider only two possible destinations for each TDM sub-wavelength signals, thus we focus on the use of 2×2 PLZT switches.
3) The *super-channel index* $\rho \in [0,P]$ is the fraction over W of requested wavelengths per input port that are randomly aggregated into couples of two adjacent wavelengths (i.e. 8×12.5 GHz bandwidth channels).
4) The *fiber switch index* $F \in [0,1]$ is the proportion over N of input ports assumed to request fiber switching in the request set. Therefore, all wavelength and super-channel channels of the input are switched to the same output. Conversely, the destination of channels that are not assumed as fiber switching is set according to a uniform distribution between the output ports. For instance, $F = 0.25$ holds for the scenario depicted in Fig. 4 since all channels fed at input 2 require to be switched to output 4.

By construction, only request sets with $\rho + \sigma \leq P$ are generated, because wavelength channels can be set either as super-channels (i.e. aggregation of two adjacent wavelengths) or carrying sub-wavelength TDM signals, but not both simultaneously.

TABLE II
AoD stages configuration for each analyzed parameter

Parameter analyzed	1st stage	2nd stage	3rd stage
P	demux	–	coupler
F	demux	–	coupler
σ	demux	PLZT	coupler

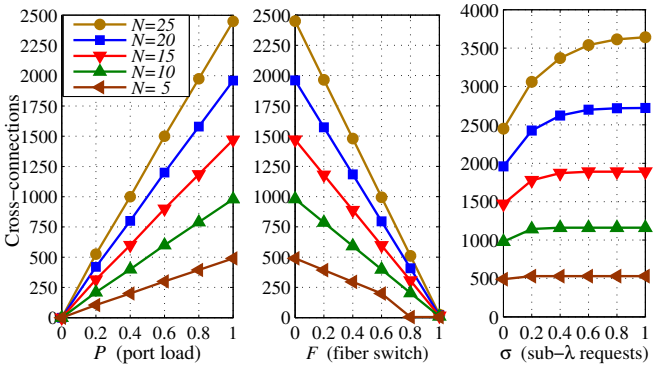

(a) $F = 0$ and $\sigma = 0$ (b) $P = 1$ and $\sigma = 0$ (c) $P = 1$ and $F = 0$

Fig. 7. Cross-connections required as a function of P, L and σ for several AoD degrees N

We focus on an off-line worst-case analysis, according to the following approach. First, we generate at random a feasible request set, based on the above traffic parameters $\{P, \sigma, \rho, F\}$. Second, starting with an AoD without any preliminary cross-connection, the AoD controller executes the proposed E-SA algorithm to design an architecture that satisfies the request set. Third, as evaluation phase, we count the required number of optical backplane cross-connections, number of components and power consumption of the designed AoD instance. We repeat this approach for 1,000 different request sets to achieve stable average results, which are reported in the following sections.

A. Scalability Analysis

We analyze the number of required cross-connections for different types of traffic requests. Note that the number of required cross-connections must be always lower than the optical backplane port-count (i.e. supported cross-connections) and thus an indicator of the scalability of the AoD.

Tab. II lists the AoD configurations used for the sensitivity analysis to the parameters P, L and σ. We consider $W = 96$ spectrum slots per fiber according to the fixed-grid DWDM standard without aggregation of adjacent wavelengths into super-channels (i.e. $\rho = 0$).

Fig. 7(a) shows the increasing behavior of the number of cross-connections with the port load P and the degree of AoD N assuming neither fiber switching requests $F = 0$ nor sub-wavelength requests $\sigma = 0$. This type of traffic requests is handled by the third step placing DEMUXs and by the coupling step of E-SA. The maximum number of required cross connections is

$$X_{DEMUX} = 2N + NW \tag{4}$$

coherently with our previous calculation in [11].

On the other hand, Fig. 7(b) shows the decreasing trend in the number of required cross-connections for traffic requests when increasing aggregation of channels in fiber switching

TABLE III
CONSUMPTION VALUES

Device	Power [W]
Common equipment	100
SSS [27]	40
Fast Switch (PLZT) [28]	8
3D-MEMS (320 p.) [30]	150

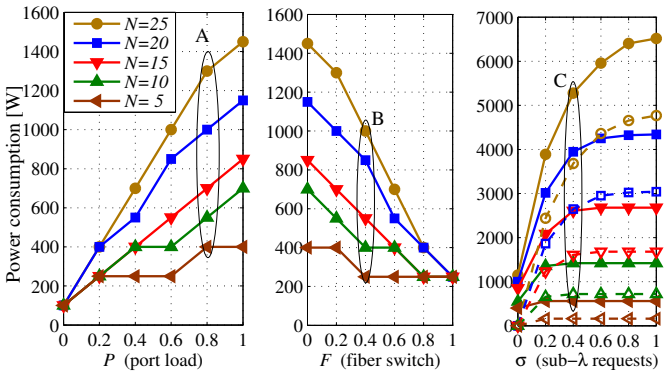

(a) $F = 0$ and $\sigma = 0$ (b) $P = 1$ and $\sigma = 0$ (c) $P = 1$ and $F = 0$

Fig. 8. Power consumption as a function of P, L and σ for several AoD degrees N

F, given a maximum load $P = 1$ and no sub-wavelength requests $\sigma = 0$. We observe a more efficient use of cross-connections, since channels can be aggregated in the first step of E-SA, thanks to fiber switching.

Fig. 7(c) shows the number of required cross-connections for request sets with sub-wavelength TDM signals σ, given a maximum load $P = 1$ and without fiber switching $F = 0$. This type of traffic requests exploits the fourth step of E-SA, which uses PLZTs and cross-connections (reusing when possible). However, the maximum number of cross-connections given by (4), for no sub-wavelength TDM requests, exceeds thousands of cross-connections. Indeed, the high number of output combinations for each sub-wavelength TDM request requires a high number of cross-connections and PLTZs, especially for high values of N.

B. Power Consumption Analysis

To evaluate the power consumption of the synthesized AoD instances, we adopt a realistic power model described by the parameters in Table III. The common equipment includes the controller, the cooling fans and the power supply. The high-speed PLZT switches are built by a switching device and a switch driver, with power consumptions in the order of few mW and 8 W, respectively. Hence, only the switch driver contribution is considered. We propose to use an *incremental power control algorithm* which turn on successive switches only when really needed. Note that this algorithm is compatible only with expandable architecture. According to the adopted realistic power model, the consumption of the AoD instance in Fig. 5(b) results to be 306 Watts.

Similarly to the scalability analysis, we consider the AoD configurations described by Tab. II for the sensitivity analysis to the parameters P, L and σ, without aggregation of adjacent wavelengths into super-channels (i.e. $\rho = 0$) and with $W = 96$ available spectrum slots per fiber.

Fig. 8(a) shows the power consumption as a function of the port load P and the degree of AoD N without fiber switching nor sub-wavelength requests. For this type of traffic requests, E-SA computes AoD instances using only, as active components, the common equipment and the backplane switches. We observe an increasing power consumption trend due to the use of additional backplane switches to provide the increasing number of required cross-connections shown in Fig. 7(a). In more detail, for $N = 25$ the number of backplane switches is 2, 4, 6, 8, and 9 for port loads $P = 0.2$, 0.4, 0.6, 0.8 and 1 respectively. This clearly shows the impact on the power consumption due to the high number of required cross-connections.

The power consumption decreases, as shown in Fig. 8(b), when the aggregation of channels into fiber switching permits a reduction in the number of backplane switches. Note that these results (as in Fig. 8(a)) are due mainly the active components being the common equipment and the backplane switches. For instance, for $N = 25$, the number of backplane switches is 9, 8, 6, 4, 2, and 1 for the reported fiber switch values respectively. This clearly shows the reduction on the power consumption due to the decreased number of required cross-connections thanks to the aggregation of channels into fiber switching. Note that different power consumption behaviors are observed in Figs. 8(a) and 8(b) depending on N due to the discrete usage of backplane switches. In particular, few increments and decrements of 150 W (i.e. one backplane switch) are observed for $N = 5$ whereas for $N = 25$ greater steps (i.e. of two backplane switches) are observed. Additionally, even if DEMUXs are not active devices, it is worth to mention that N DEMUXs are used under traffic conditions of Fig. 8(a) whereas a linear reduction on their number is observed in Fig. 8(b) as F increases.

Fig. 8(c) shows the power consumption as a function of the sub-wavelength requests σ, without fiber switching requests $F = 0$, with maximum load $P = 1$ and with N as parameter. The AoD instances obtained by the E-SA under these traffic conditions use as active components the common equipment, the backplane switches, and the PLZT switches. Thus, white symbols and dashed lines show the power consumption of the used PLZTs, while the remainder power consumption belongs to the common equipment and the backplane switches. For smaller N, the power consumption is mainly due to the common equipment and backplane switches. However, as N and σ increase, PLZTs become the major contributor to total power consumption. Indeed, note that for this type of traffic requests the number of cross-connections (shown in Fig. 7(c)) increases at a lower pace with respect to the power consumption. Let us consider the number of devices used by the synthesized AoDs for $N = 25$ under the traffic conditions of Fig. 8(c). On the one hand, the number of backplane switches is 8, 10 and 11, for the sub-wavelength requests $0 \leq \sigma \leq 0.4$, and 12 for $\sigma \geq 0.6$ respectively. On the other hand, the number of 2×2 PLZT switches are 300, 470, 540, 580 and 600 for the sub-wavelength requests $\sigma \geq 0.2$ respectively (no PLZT switches are used for $\sigma = 0$). We observe a clear increase on both the number of backplane and PLZT switches for low values of σ due to the number of possible combinations to be switched towards the $N = 25$ output ports. However, as σ increases, i.e. $\sigma \geq 0.6$, the number of remaining outputs that can be used as possible destinations decreases, limiting the increase trend on number of both switches. This behavior is more evident for lower number of N where a constant number of both switches is used above lower values of σ (e.g. $\sigma \geq 0.4$ for $N = 15$).

TABLE IV
WAVELENGTH/SUPER-CHANNEL DECOMPOSITION AND CORRESPONDING THROUGHPUT ACHIEVED IN FIG. 9

ρ	Wavelength channels*	Super-channels**	Throughput per port (Tb/s)	Throughput in Tb/s
0	96	0	9.6	240
0.2	78	9	11.4	285
0.4	60	18	13.2	330
0.6	40	28	15.2	380
0.8	20	38	17.2	430
1	0	48	19.2	480

* 100Gb/s in 4×12.5 GHz ** 400Gb/s in 8×12.5 GHz

C. Migration Towards Flexible-Grid Spectrum

We analyze the AoD scalability under traffic requests that aggregate spectrum slots into super-channels, according to the parameter ρ. We consider such aggregated traffic as the migration from fixed-grid spectrum (i.e. with well defined DWDM 96 fixed-grid spectrum slots of size 4×12.5 GHz) towards flexible grid where super-channels are considered as set of adjacent spectrum slots placed arbitrarily in the spectrum occupying 8×12.5 GHz. This approach complies with the flexible grid definition given by the ITU-T recommendation G.694.1 (i.e. nominal central frequency granularity of 6.25 GHz and slot width granularity of 12.5 GHz). Indeed, the arbitrary spectral placement of wavelength and super-channels is not possible with fixed-grid optical spectrum switching. In particular, arbitrary placement of aggregates of wavelengths (i.e. super-channels) and fixed-grid wavelengths prevents the use of fixed-grid AWG-based (DE)MUXs. Therefore, the arbitrary spectrum switching of spectrum selective switches is required (e.g. see input 1 in Fig. 4(a) requiring the SSS).

The second and third column of Tab. IV lists the decomposition in single wavelength and super-channels for the different values of ρ, assuming maximum load $P = 1$. For single wavelength channels in fixed grid with 4×12.5 GHz slots, DP-QPSK at 100Gb/s is considered, whereas for super-channels in flexible grid with 8×12.5 GHz slots, the spectral efficiency of the super-channels is assumed to be twice that of 100 Gb/s DP-QPSK, thanks to the use of more efficient modulation formats, e.g. DP-16QAM. Thus, given the 4.8 THz available in the C band, 96 DP-QPSK channels at 100 Gb/s are considered for $\rho = 0$. As ρ increases, the number of requested super-channels at 400 Gb/s increases up to 48 channels for $\rho = 1$ (i.e. full flexible grid). Therefore, the AoD throughput in the flex grid is twice as compared with the fixed-grid case. The flexible-grid approach may impact the reachable distance by the optical signal [32]. However, we consider suitable a transponder reach of 800 km for the DP-16QAM at 400 Gb/s bitrate, whose feasibility is shown in [2].

Fig. 9(a) shows the number of required cross-connections for AoD with degree $N = 25$, traffic requests with full load $P = 1$, no TDM sub-wavelength signals and different levels of aggregation in fiber switching F and in super-channels ρ. E-SA designs the AoD instances with DEMUXs in the first stage and couplers in the third stage, for traffic requests with no aggregation in super-channels. When wavelengths are aggregated together in super-channels (as ρ increases) DEMUXs in the first stage are progressively replaced by SSSs. Note that the number of cross-connections is given by (4) for the fixed-grid scenario ($\rho = 0$) and decreases as the aggregation in fiber switching increases, as already shown in Fig. 7(a). When super-channel requests are introduced ($\rho > 0$), the number of cross-connections is reduced by half for the $F = 0$ case. This is due to the capability of the SSSs to switch several spectrum slices over a single port. For $\rho = 1$ (i.e. full flexible grid) the number of cross-connections is slightly below

$$X_{SSS} = 2N + N^2 \tag{5}$$

which allows a reduction of 75% when all DEMUXs are replaced by SSSs. In more detail, the maximum number of cross-connections given by (5) is an upper bound because, in most of the cases, a full-mesh between input and output ports is not required.

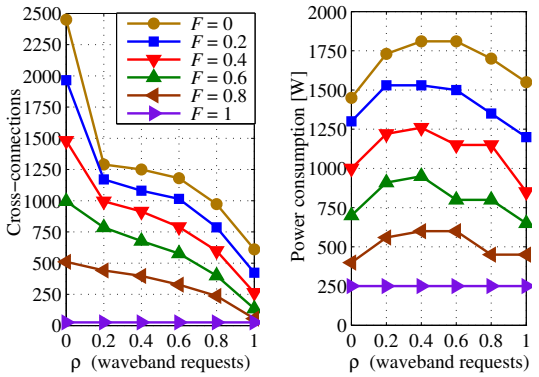

(a) $P = 1$ and $\sigma = 0$ (b) $P = 1$ and $\sigma = 0$

Fig. 9. (a) Required cross-connections and (b) power consumption for an AoD degree $N = 25$ as a function of fiber switch F and super-channel requests ρ

As shown in Fig. 9(b), a reduction of the power consumption is experienced as F increases, since fewer backplane switches are used, thanks to the aggregation of channels due to fiber switching. However, when super-channel requests are introduced ($\rho > 0$), higher power consumption is experienced due to the partial replacement of passive DEMUXs by active SSSs. In particular, for $0.2 \leq \rho \leq 0.8$, a combination of a high number of optical backplane switches (due to a large number of cross-connections required by DEMUXs) and SSSs leads to a higher power consumption compared to either $\rho = 0$ or $\rho = 1$. For $\rho = 1$, the first stage of the AoD node is composed only of SSSs and three optical backplane switches are used (more precisely, only one for $F \geq 0.35$). Hence, a lower power consumption is experienced with respect to the case $0.2 \leq \rho \leq 0.8$.

We analyze the impact of the degree N for the migration towards flexible-grid spectrum in terms of required cross-connections in Fig. 10(a) and we report the corresponding power consumption in Fig. 10(b). In more detail, Fig. 10 analyzes AoD instances under traffic requests with full load $P = 1$, no TDM sub-wavelength signals and different levels of aggregation in super-channels ρ for different values of N. We observe similar trends comparing here the degree of AoD with the aggregation into fiber switching in Fig. 9. However, note that the results reported in Fig. 9(b), correspond to different power consumptions for traffic requests with increasing values of aggregation into fiber switching (i.e. being the maximum $N = 25$ for $F = 0$), whereas Fig. 10(b) reports the maximum power consumption values for different values of N. Indeed, note that the highest power consumption values correspond to the same traffic requests:

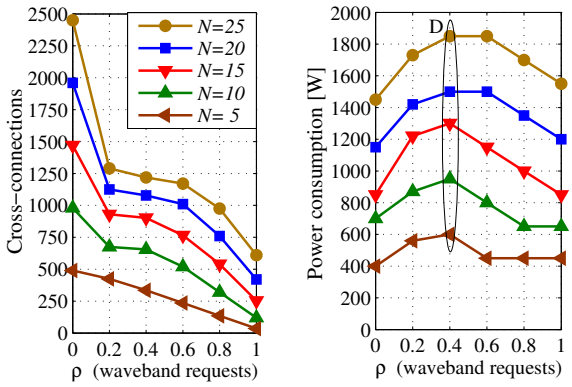

(a) $P = 1, \sigma = 0$ and $F = 0$ (b) $P = 1, \sigma = 0$ and $F = 0$

Fig. 10. (a) Cross-connections and (b) power consumption as a function of super-channel requests ρ for several AoD degrees N

$N = 25$, $P = 1$, $\sigma = 0$, $F = 0$ and $0 \leq \rho \leq 1$. In more detail, for $N = 25$ and $\rho = 0$, now 9 backplane switches are used to establish all the required cross-connections by the DEMUXs, whereas only 3 backplane switches and 25 SSSs are used for $\rho = 1$. However, as in Fig. 9(b), for $0.2 \leq \rho \leq 0.8$, a combination of a high number of optical backplane switches and SSSs leads to a higher power consumption compared to either $\rho = 0$ or $\rho = 1$.

In summary, in our considered scenarios, the migration from fixed grid to flexible grid offers 75% cross-connection reduction, doubles the AoD node throughput while keeping a similar power consumption.

D. Comparison of AoD with ROADMs

Here we compare the power consumption and the cost of AoD with other ROADM architectures reported in the literature. To this aim, Tab. V shows the required number of devices to implement several architectures proposed in the literature. We consider 25% as add/drop ratio per port. Note that we denote architectures #1 to #4 with the original numeric ID of [3]. The C/D/C-ROADM architecture #5 reported in [4] is based on the same structure of #2.

1) Power consumption comparison: Tab. VI lists different traffic conditions given by $\{P, F, \sigma, \rho\}$ and denoted as traffic *setups* {A, B, C, D, E, F}. Note that traffic setups {A, B, C, D} extend the power consumption results presented in Fig. 8 and Fig. 10(b). In particular, setup A explores the power consumption of AoD for a fixed-grid wavelength traffic load of 80%. Setups B, C and D explore the power consumption of AoD for a traffic loaf of 100% with different fractions of sub-wavelength, super-channel and fiber requests respectively. Finally, setups E and F explore the power consumption of AoD for a traffic load of 100% and with aggregation into super-channel and fiber requests.

Fig. 11 compares the power consumption for the different architectures in Tab. V with AoD under the traffic setups of Tab. VI. All the considered setups for AoD require a lower power consumption than the architectures proposed in the literature. Furthermore, time switching can be supported in AoD, unlike other architectures. However, when such capability is exploited, a higher power consumption is experienced, as shown by setup C.

Notably, the inherent flexibility of AoD permits to save power when compared to other architectures. Power savings depend on both the aggregation into fiber switching and into super-channels. For instance, more than 60% power consumption reduction is achieved in setup B due to traffic aggregation into fiber switching compared to architecture #3. However, as shown in setup D, only 20% of power consumption reduction is obtained for aggregation into super-channel only. Higher power consumption savings are obtained when aggregation into fiber switching and into super-channels are combined together (i.e. 50% and 75% of power consumption reduction for setups E and F respectively depicted with dashed lines).

The ability to switch at different levels (fiber, flex-grid super-channel and fixed-grid wavelength) reduces the number of required SSS modules and optical switches saving their associated power consumption. Therefore, power consumption savings are obtained for AoD depending on the traffic supported (except when time-sliced sub-wavelengths are supported) thanks to the adaptable nature of the architecture. Note that such adaptation to the traffic is obviously not possible with hard-wired ROADMs. Finally, it is worth to mention that configuration times for AoD and ROADMs are similar due to use of sub-systems with similar configuration times. Therefore, AoD nodes do not present configuration time issues nor penalties compared to ROADMs, and in any case, configuration or synthesis procedures (as the E-SA in Sec. IV) are not related to power consumption.

2) Cost comparison: Tab. VII lists the cost in arbitrary units for different devices considering as reference the price of a 40-channel Array Waveguide Grating (AWG)-based (DE)MUXs. The reported costs are based on confidential information given by the different manufacturers. Note that since PLZT switches are not a mature technology [28], we have considered its cost per port notably higher than for the OXC case based on 3D-MEMS. Similarly, since SSSs are currently targeting research purposes, we have considered their cost 20% higher than the cost of commercially available Wavelength Selective Switches (WSSs). Moreover, we consider that future SSS will have 25 ports as current prototypes of WSS. The cost of couplers/splitters are not considered in this analysis since it is negligible compared

TABLE V
NUMBER OF DEVICES FOR DIFFERENT ARCHITECTURES

Arch.	**Active comp.**			**Passive comp.**	
	SSS	3D-MEMS*	Switch**	(de)Mux	Splitter
#1 [3]	0	$1\times\{3NW\}$	0	$2N$	0
#2 [3]	N	0	$NW/2$	0	$2N$
#3 [3]	N	$1\times\{NW\}$	0	$2N$	N
#4 [3]	$2N$	$2\times\{NW\}$	0	0	$3N$
#5 [4]	N	0	$NW/2$	0	$2N$
#6 [5]	N	$2\times\{NW\}$	0	N	N

* Num. slow switches $\times\{$size$\}$ **Num. fast switches $1\times N$

TABLE VI
TRAFFIC PARAMETERS FOR EACH *setup*

Setup	P	F	σ	ρ
A	0.8	0	0	0
B	1	0.4	0	0
C	1	0	0.4	0
D	1	0	0	0.4
E	1	0.4	0	0.4
F	1	0.8	0	0.4

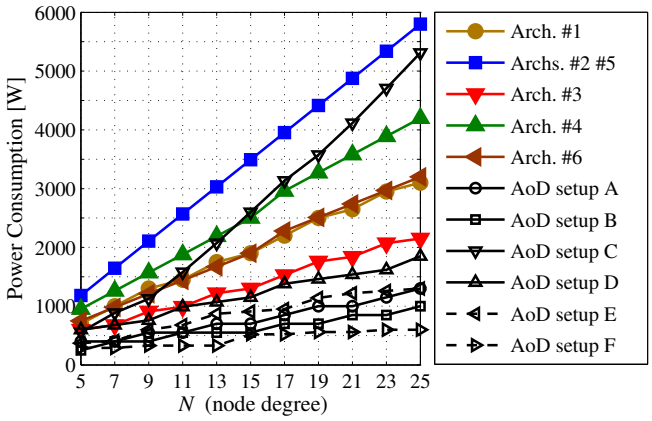

Fig. 11. Power consumption comparison between AoD and different ROADM architectures reported in the literature

to the other reported costs.

The cost of the different ROADMs proposed in the literature is obtained according to their number of devices reported in Tab. V and considering $W = 96$ spectrum slots. For the number of OXCs, in the case that the size of the 3D-MEMS (i.e. number of ports) required by the ROADM architecture exceeds 320 (considering commercially available 320-port 3D-MEMS switch [30]) the number of 3D-MEMS switches is obtained by interconnecting switches similarly as for the AoD case (3). Note that Tab. V shows the number of required ports by the 3D-MEMS switches for the different ROADMs which is $3NW$ for architecture 1 and NW for architectures 3, 4, and 6, respectively.

AoD is dimensioned for this cost comparison analysis considering the required devices for maximum load $P = 1$ and no aggregation into fiber switching $F = 0$. Indeed, unlike the power consumption comparison, here we dimension AoD for the cases in which the maximum number of devices are required. In other words, no cost can be saved when devices connected to the backplane are not used due particular traffic conditions. However, beyond such worst case analysis that take into account previous results for the number of devices, AoD can follow a pay-as-you-grow cost model since the devices used are not correlated with neither the bypass in/out fibers nor the transponders for add/drop traffic. Three different AoD dimensioning cases are considered for this cost comparison:

1) AoD *fixed* grid: This case considers an AoD deployment in a legacy network with fixed-grid spectrum of $W = 96$ slots. In particular, it consists of a first stage with a DEMUX per input port, a third stage of couplers, and thus a number of cross-connections (4).
2) AoD *flexible* grid: Here we consider an AoD deployment in a future network that has migrated to a flexible-grid spectrum allocation. Therefore, the deployed AoD consists of a first stage with a SSS per input port, a third stage of couplers, and therefore a number of cross-connections (5).
3) AoD *sub-*λ: This case contemplates an AoD deployment in a long-term future network capable to support at maximum 20% of the total traffic containing TDM sub-wavelength requests. The AoD considered in this case consists of a first stage with a SSS per input port, a second stage with a number of PLZTs according to $\sigma = 0.2$ in Fig. 8(c), a third stage of couplers, which results on a number of cross-connections higher than (5) due to the use of the PLZTs at the second stage.

TABLE VII
COST VALUES

Device	Cost [a.u.]
Mux/demux 40 channels	1
Mux/demux 96 channels	1.8
PLZT 2×2 ports	2
WSS 1×5 ports	4.5
WSS 1×9 ports	5.5
WSS 1×20 ports	9.5
OXC 320 ports	55
SSS 1×25 ports	1.2 × WSS

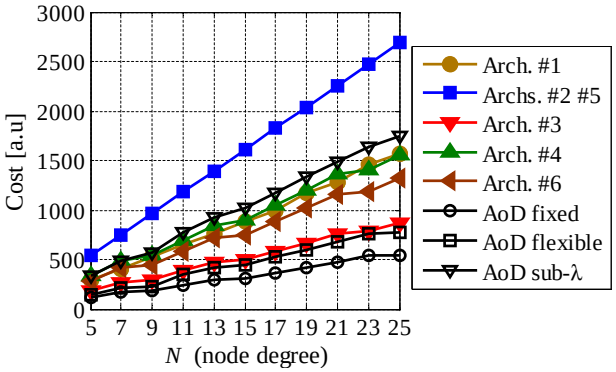

Fig. 12. Cost comparison between AoD and different ROADM architectures reported in the literature

The number of backplane switches required is obtained according to (3) for the three considered cases. Similarly as in the power consumption comparison, we consider 25% as add/drop ratio per port.

Fig. 12 compares the cost for the different ROADM architectures listed in Tab. V with AoD for the dimensioning cases previously referred. We observe several similarities between the cost comparison and the power comparison in Fig. 11. In particular, architectures #2 and #5 exhibit the highest cost due to the use of PLZT switches. On the other hand, architecture #3 presents the lowest cost among the different ROADMs achieving a comparable cost with the fixed- and flexible-grid spectrum AoD cases. Moreover, when TDM sub-wavelength traffic is considered for the deployment of AoD, the overall cost becomes higher than several of the ROADMs considered. Indeed, similar observation holds for the power consumption when the TDM sub-wavelength switching capability is exploited by AoD.

The reader may refer to [33] for a more detailed cost analysis on AoD, its comparison against ROADMs, and its impact on network-wide scenarios.

VI. AoD High-Capacity Alternatives

We explore two different scenarios for AoD to support high-capacity optical switching. In the first scenario, we consider a wide available spectrum which consists of C and L bands according to the ITU-T recommendation [29]. Indeed, recent developments on RAMAN-based optical amplifiers permit the use of three additionally available spectrums compared to traditional EDFA-based amplifiers [34]. In the second scenario, we consider an increment on the spatial

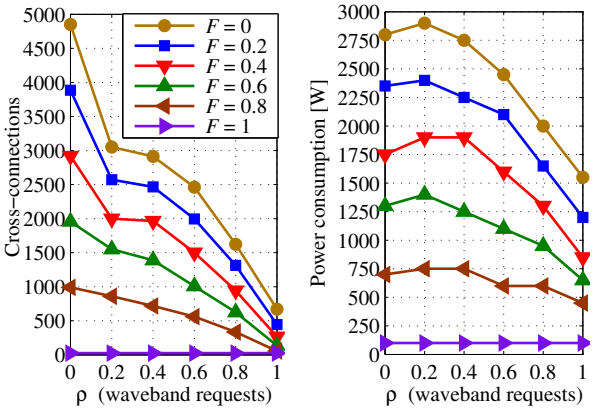

(a) $P = 1$ and $\sigma = 0$ (b) $P = 1$ and $\sigma = 0$

Fig. 13. (a) Required cross-connections and (b) power consumption for an AoD degree $N = 25$ and $W = 192$ as a function of fiber switch F and super-channel requests ρ

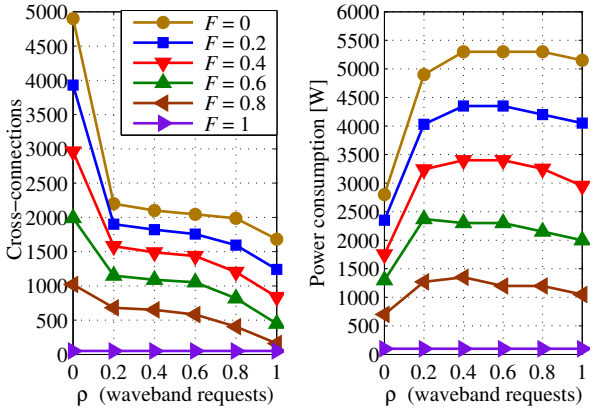

(a) $P = 1$ and $\sigma = 0$ (b) $P = 1$ and $\sigma = 0$

Fig. 14. (a) Required cross-connections and (b) power consumption for an AoD degree $N = 50$ and $W = 96$ as a function of fiber switch F and super-channel requests ρ

dimension exploring the performance of a high degree AoD node. Subsequently, we compare both spectrum and space high-capacity alternatives. Traffic requests do not contain TDM sub-wavelength signals.

A. *Extended Spectrum (C plus L bands)*

As first scenario, we consider a wide available spectrum which consists of C and L bands, leading to $W = 192$ available spectrum slots. Fig. 13(a) shows the number of required cross-connections for AoD with $N = 25$, traffic requests with full load $P = 1$ and different levels of aggregation in fiber switching F and in super-channels ρ. Similarly to Sec. V-C, AoD instances with DEMUXs in the first stage are synthesized for traffic requests with no aggregation in super-channels, whereas when ρ increases, i.e. wavelengths are aggregated together in super-channels, DEMUXs are progressively replaced by SSSs. We consider a single SSS per input port at the first stage able to switch arbitrarily the entire C and L bands. Similarly to the results obtained in Fig. 9(a), the number of cross-connections given by (4) for the fixed-grid scenario ($\rho = 0$) decreases as the aggregation in fiber switching increases. However, still comparing with Fig. 9(a), a higher reduction in the number of cross-connections can be observed for high values of aggregation of wavelengths in super-channels ($\rho \geq 0.6$). Indeed, for $\rho = 1$ and $F = 0$, the number of cross-connections has the upper bound given by (5), which allows a reduction in number of cross-connections of 86% when all DEMUXs are replaced by SSSs.

Regarding the power consumption of these wide-spectrum traffic requests, we observe in Fig. 13(b) similar trends as in Fig. 9(b) when F increases. However, when the number of super-channel requests increases, the power consumption is reduced more rapidly than for the $W = 96$ case. Indeed, thanks to the aggregation in super-channels and the arbitrary bandwidth switching capability of the SSSs, we obtain the same power consumption as in Fig. 9(b) for $\rho = 1$.

B. *Large Number of AoD Node Degrees*

As second scenario, we explore the AoD performance in terms of required cross-connections and power consumption when E-SA synthesizes high port-count architectures. To this aim, Figs. 14(a) and 14(b) show the number of required cross-connections and power consumption respectively for an AoD node with degree $N = 50$, traffic requests with full load $P = 1$ and different levels of aggregation in fiber switching F and in super-channels ρ. As previously, AoD instances with DEMUXs in the first stage are synthesized for traffic requests with no aggregation in super-channels, whereas when ρ increases, DEMUXs are progressively replaced by SSS-based composed modules. We consider that future SSS will have 25 ports as current prototypes of Wavelength Selective Switches (WSS). Therefore, to achieve switching towards 50 different node degrees, we consider a composed module per input port at the first stage which includes a 1×2 splitter and two SSSs to provide connectivity towards the third stage modules.

We observe in Fig. 14(a) a linear reduction of the number of cross-connections as the aggregation in fiber switching increases and a drastic reduction when super-channels requests are introduced, similar to the $N = 25$ and $W = 96$ case depicted in Fig. 9(a). However, high values of ρ do not provide additional reduction on the number of required cross-connections. Indeed, the high degree considered in this case limits the switching capability of the SSSs because more space than spectrum switching has to be supported. On the other hand, we observe in Fig. 14(b) a notable increase on the power consumption when super-channel requests are introduced. For instance, the use of two SSSs per port (i.e. 100 SSSs total) implies a power consumption of 4,000 W for the case without aggregation in fiber switching ($F = 0$). Indeed, this poses a severe limitation to high-degree solutions.

C. *Trade-offs between High-Capacity Alternatives*

Tab. VIII summarizes the different high-capacity alternatives in terms of required cross-connections (denoted as "xc"), required power consumption in Watts and achieved throughput in Tb/s. Results obtained in Sec. V-C are also listed for comparison purposes. The reported summary table coincides with the $F = 0$ curves (no aggregation in fiber switching) of Figs. 9, 13 and 14 in each row respectively.

Both wide-spectrum and high-degree scenarios provide twice the throughput compared to the standard AoD limited

TABLE VIII
SUMMARY OF DIFFERENT HIGH-CAPACITY ALTERNATIVES

Scenario	ρ					
	0	0.2	0.4	0.6	0.8	1
N = 25	2450 xc	1295 xc	1253 xc	1181 xc	973 xc	610 xc
W = 96	1450 W	1730 W	1810 W	1810 W	1700 W	1550 W
	240 Tb/s	285 Tb/s	330 Tb/s	380 Tb/s	430 Tb/s	480 Tb/s
N = 25	4850 xc	3053 xc	2912 xc	2461 xc	1623 xc	669 xc
W = 192	2800 W	2900 W	2750 W	2450 W	2000 W	1550 W
	480 Tb/s	570 Tb/s	660 Tb/s	760 Tb/s	860 Tb/s	960 Tb/s
N = 50	4900 xc	2207 xc	2102 xc	2045 xc	1987 xc	1680 xc
W = 96	2800 W	4900 W	5300 W	5300 W	5300 W	5150 W
	480 Tb/s	570 Tb/s	660 Tb/s	760 Tb/s	860 Tb/s	960 Tb/s

to C band and up to 25 node degrees. Furthermore, also both high-capacity cases require almost twice the number of cross-connections and power consumption if compared to the standard AoD configuration when no aggregation into super-channel is requested (i.e. $\rho = 0$). Note that for traffic requests with $0.2 \leq \rho \leq 0.6$, where a combination of wavelengths and super-channels is used, the scenario with extended spectrum (i.e. C plus L bands) requires more than twice the number of cross-connections and higher power consumption than the standard case. This is due to the high number of wavelengths that needs demultiplexing and subsequent multiplexing, which consequently requires a high number of ports, i.e. larger optical backplane. Nevertheless, as the fraction of super-channel switching increases, the number of cross-connections and the power consumption drop to similar values as in the standard AoD case. This reduction is achieved as SSSs utilize a single port to switch multiple wavelengths and super-channels, which is not possible with passive optical (de)multiplexers. Therefore, for the extended spectrum scenario it is beneficial to implement (de)multiplexing functions using SSS rather than passive wavelength (de)mux devices.

The high-degree AoD scenario shows a slight reduction in the number of required cross-connections compared to the extended spectrum scenario for super-channel switching within the range $0.2 \leq \rho \leq 0.6$. However, it also implies a higher power consumption because a larger number of active SSSs is required. Therefore, these results show that the extended spectrum scenario should be preferred to the high AoD degree alternative. Nevertheless, the extended spectrum scenario requires SSS devices that support both the C and L bands, whereas the large AoD degree scenario requires devices that support only the C band.

VII. CONCLUSIONS

We studied the power consumption and backplane cross-connections scalability of AoD, supporting TDM sub-wavelength, wavelength, super-channels and fiber switching. First, we presented the Enhanced Synthesis Algorithm to automatically design AoD instances according to the traffic request. Then, we reported a scalability and power consumption analysis under different profiles of traffic requests. Furthermore, we showed the benefits of traffic grooming in super-channel switching and the impact of the arbitrary bandwidth switching capability provided by the SSSs at the AoD node level. Our results show that the adaptability of AoD offers significant power saving compared to other architectures unless power-demanding functionalities (e.g. time switching) are supported. In addition, our results indicate that AoD worst case cost is better or comparable to traditional ROADM architectures. Moreover, its pay-as-you-grow modular and flexible nature (plug-in modules with diverse functionalities) disassociated from the degrees of architecture provides considerable benefits. Finally, we showed the convenience of enabling additional spectrum switching rather than providing additional space switching, considering SSS devices that support both C and L bands. In conclusion, the high flexibility offered by AoD brings considerable power efficiency to the optical node while providing a throughput of hundreds of Tb/s.

ACKNOWLEDGMENTS

The authors thank the financial support of FUNTTEL, FINEP, CPqD Foundation under the project 100GETH, the EC FP7 grant agreement No. 317999 IDEALIST, and the EPSRC grant EP/I01196X: The Photonic Hyperhighway.

REFERENCES

[1] O. Gerstel, M. Jinno, A. Lord, and S.J.B. Yoo, "Elastic optical networking: A new dawn for the optical layer?", *IEEE Communications Magazine*, **50**(2), pp.12–20, 2012.

[2] C. Politi, V. Anagnostopoulos, C. Matrakidis, and A. Stavdas, "Routing in dynamic future flexi-grid optical networks", *Optical Network Design and Modeling (ONDM)*, pp. 1–4, 2012.

[3] P. Ji and Y. Aono, "Colorless and directionless multi-degree reconfigurable optical add/drop multiplexers", *Wireless and Optical Communications Conference (WOCC)*, pp. 1–5, May 2010.

[4] S. Gringeri, B. Basch, V. Shukla, R. Egorov, T.J. Xia, "Flexible architectures for optical transport nodes and networks", *IEEE Communications Magazine*, **48**(7), pp. 40–50, July 2010.

[5] R. Jensen, "Optical switch architectures for emerging colorless/directionless/contentionless ROADM networks", *Optical Fiber Communication Conference (OFC)*, 2011.

[6] J. Berthold, A. A. M. Saleh, L. Blair, and J. M. Simmons, "Optical networking: past, present, and future", *Journal of Lightwave Technology (JLT)*, vol. 26, n. 9, May 2008.

[7] A. Autenrieth, A.K. Tilwankar, C.M. Machuca, and J.P. Elbers, "Power consumption analysis of opaque and transparent optical core networks", *International Conference on Transparent Optical Networks (ICTON)*, pp. 1–5, 2011.

[8] M. Murakami, and K. Oda, "Power consumption analysis of optical cross-connect equipment for future large capacity optical networks", *International Conference on Transparent Optical Networks (ICTON)*, pp. 1–4, 2009.

[9] N. Amaya, G. Zervas, and D. Simeonidou, "Architecture on demand for transparent optical networks", *International Conference on Transparent Optical Networks (ICTON)*, pp. 1–4, 2011.

[10] N. Amaya, G. Zervas, and D. Simeonidou. Introducing Node Architecture Flexibility for Elastic Optical Networks, *Journal of Optical Communications and Networking (JOCN)*, vol. 5, pp. 593–608, 2013.

[11] M. Garrich, N. Amaya, G. Zervas, P. Giaccone and D. Simeonidou, "Architecture on Demand: Synthesis and Scalability", *Optical Network Design and Modeling (ONDM)*, pp. 1–6, 2012.

[12] M. Garrich, N. Amaya, G. Zervas, P. Giaccone and D. Simeonidou, "Power consumption analysis of Architecture on Demand", *European Conference on Optical Communication (ECOC)*, 2012.

[13] E. B. Basch, R. Egorov, S. Gringeri and S. Elby, "Architectural tradeoffs for reconfigurable dense wavelength-division multiplexing systems", *Journal of Selected Topics in Quantum Electronics*, vol. 12, no. 4, pp. 615-626, July 2006.

[14] V. Kaman, R. J. Helkey and J. E. Bowers, "Multi-degree ROADMs with agile add-drop access", *Photonics in Switching*, Aug. 2007.

[15] V. Kaman, S. Yuan, O. Jerphagnon, R. J. Helkey and J. E. Bowers, "Comparison of wavelength-selective cross-connect architectures for reconfigurable all-optical networks", *Photonics in Switching*, Oct. 2006.

[16] S. Thiagarajan, L. Blair and J. Berthold, "Direction-independent add/drop access for multi-degree ROADMs", *Optical Fiber Communication/National Fiber Optic Engineers Conference*, Feb. 2008.
[17] T. Watanabe, K. Suzuki, T. Goh, K. Hattori, A. Mori, T. Takahashi, and S. Kamei, "Compact PLC-based transponder aggregator for colorless and directionless ROADM", *Optical Fiber Communication Conference (OFC)*, 2011.
[18] W. Way, "Optimum architecture for MN multicast switch-based colorless, directionless, contentionless, and flexible-grid ROADM", *Optical Fiber Communication Conference (OFC)*, 2012.
[19] T. Watanabe, S. Kenya, and T. Takahashi, "Silica-based PLC transponder aggregators for colorless, directionless, and contentionless ROADM", *Optical Fiber Communication Conference (OFC)*, 2012.
[20] R. Younce, J. Larikova, and Y. Wang, "Engineering 400G for Colorless-Directionless-Contentionless Architecture in Metro/Regional Networks", *Journal of Optical Communications and Networking (JOCN)*, vol. 5, no. 10, pp. A267–A273, Oct. 2013.
[21] E.C. Magalhes, et al., "Node Architectures for Next Generation ROADMs: A comparative study among emergent optical solutions", *Journal of Microwaves, Optoelectronics and Electromagnetic Applications (JMOe)*, v.12, SI.2, www.jmoe.org, July 2013.
[22] N. Amaya, M. Irfan, G. Zervas, K. Banias, M. Garrich, I. Henning, D. Simeonidou, Y. R. Zhou, A. Lord, K. Smith, V. J. F. Rancano, S. Liu, P. Petropoulos, and D. J. Richardson, "Gridless optical networking field trial: Flexible spectrum switching, defragmentation and transport of 10G/40G/100G/555G over 620-km field fiber", *Optics Express*, pp. B277–B282, 2011.
[23] N. Amaya, M. Irfan, G. Zervas, R. Nejabati, D. Simeonidou, J. Sakaguchi, W. Klaus, B.J. Puttnam, T. Miyazawa, Y. Awaji, N. Wada, I. Henning, "First fully-elastic multi-granular network with space/frequency/time switching using multi-core fibres and programmable optical nodes", *Optics Express*, vol. 21, issue 7, pp. 8865–8872, Apr. 2013.
[24] N. Amaya, et al., "First Demonstration of Software Defined Networking (SDN) over Space Division Multiplexing (SDM) Optical Networks", *European Conference on Optical Communication (ECOC)*, 2013.
[25] B. R. Rofoee, G. Zervas, Y. Yan, N. Amaya, and D. Simeonidou, "All Programmable and Synthetic Optical Network: Architecture and Implementation", *Journal of Optical Communications and Networking (JOCN)*, vol.5, no.9, pp.1096–1110, June 2013.
[26] M. Dzanko, B. Mikac, N. Amaya, G. Zervas, and D. Simeonidou, "Availability analysis of optical cross-connect implemented by architecture on demand", *Int. Conf. in Transparent Optical Networks (ICTON)*, 2012.
[27] Finisar's Waveshaper, http://www.finisar.com/
[28] K. Nashimoto, D. Kudzuma, and H. Han, "High-speed switching and filtering using PLZT waveguide devices", *OptoeElectronics and Communications Conference (OECC)*, pp. 540–542, 2010.
[29] ITU-T G.694.1, "Spectral grids for WDM applications: DWDM frequency grid", http://www.itu.int/rec/T-REC-G.694.1-201202-I/en
[30] Calient's FiberConnect, http://www.calient.net/products/
[31] M. Garrich, E. Magalhaes, H. Carvalho, A. Bianco, P. Giaccone, G. Zervas, D. Simeonidou, N. Gonzalez, J. Oliveira, and J. Oliveira, "Experimental Demonstration of Backplane Architectures for Programmable Optical Nodes," *European Conference on Optical Communication (ECOC)*, 2014.
[32] M. Jinno, B. Kozicki, H. Takara, A. Watanabe, Y. Sone, T. Tanaka, and A. Hirano, "Distance-adaptive spectrum resource allocation in spectrum-sliced elastic optical path network", *IEEE Communications Magazine*, **48**(8), pp. 138–145, 2010.
[33] A. Muhammad, G. Zervas, N. Amaya, D. Simeonidou, and R. Forchheimer, "Introducing Flexible and Synthetic Optical Networking: Planning and Operation Based on Network Function Programmable ROADMs," *Journal of Optical Communications and Networking (JOCN)*, v. 6, n. 7, pp. 635-648, 2014.
[34] G. Charlet, M. Salsi, P. Tran, M. Bertolini, H. Mardoyan, J. Renaudier, O. Bertran-Pardo, and S Bigo, "72×100Gb/s transmission over transoceanic distance, using large effective area fiber, hybrid Raman-Erbium amplification and coherent detection", *Optical Fiber Communication (OFC)*, 2009.